Crystal Engineering, Electron Conduction, Molecular Recognition and Reactivity by Chalcogen Bonds in Tetracyanoquinodimethanes Fused with [1,2,5]Chalcogenadiazoles

Takuya Shimajiri, Henri-Pierre Jacquot de Rouville, Valérie Heitz, Tomoyuki Akutagawa, Takanori Fukushima, Yusuke Ishigaki, Takanori Suzuki

Crystal Engineering, Electron Conduction, Molecular Recognition and Reactivity by Chalcogen Bonds in Tetracyanoquinodimethanes Fused with [1,2,5]Chalcogenadiazoles

Takuya Shimajiri[a,b]
Henri-Pierre Jacquot de Rouville[c]
Valérie Heitz[c]
Tomoyuki Aktagawa[d]
Takanori Fukushima[e]
Yusuke Ishigaki[a]
Takanori Suzuki*[a]

[a] Department of Chemistry, Faculty of Science, Hokkaido University, Sapporo, Hokkaido 060-0810, Japan
tak@sci.hokudai.ac.jp

[b] Creative Research Institution, Hokkaido University, Sapporo, Hokkaido 001-0021, Japan

[c] Laboratoire de Synthèse des Assemblages Moléculaires Multifonctionnels, Institut de Chimie de Strasbourg, CNRS UMR 7177, Université de Strasbourg, 4, rue Blaise Pascal, 67000 Strasbourg, France

[d] Institute of Multidisciplinary Research for Advanced Materials, Tohoku University, Sendai, Miyagi 980-8577, Japan

[e] Laboratory for Chemistry and Life Science, Institute of Innovative Research, Tokyo Institute of Technology, Yokohama 226-8503, Japan

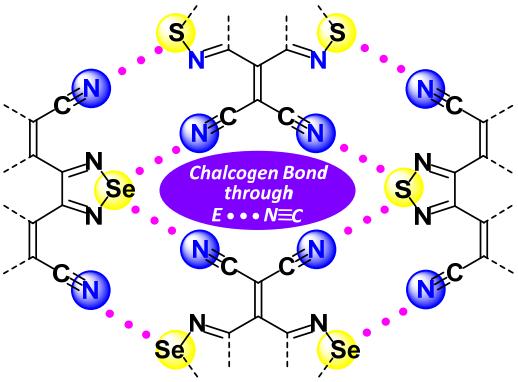

Received:
Accepted:
Published online:
DOI:

Abstract Studies on a series of tetracyanoquinodimethanes (TCNQs) fused with [1,2,5]chalcogenadiazole rings revealed that chalcogen bonds (ChB) through E ••• N≡C (E = S or Se) contacts are a decisive factor in determining their crystal structures, with the formation of one- or two-dimensional networks in a lateral direction. For anion-radical salts generated by one-electron reduction, electron conduction occurs in the direction of the network due to intermolecular electronic interaction by ChB. Based on the reliable synthon of E ••• N≡C for crystal engineering, molecular recognition occurs so that solid-state molecular complexes are selectively formed with certain donors, such as xylenes, among their isomers by charge-transfer-type clathrate formation. The inclusion cavity of the clathrate could provide a reaction environment for photoinduced electron-transfer in the solid state. The accommodation of multiple conformers of overcrowded ethylene exhibiting thermo/mechanochromism is another example of the novel functions that can be realized by ChB through E ••• N≡C contacts. Therefore, these chalcogenadiazolo-TCNQs endowed with the ability to form ChB are promising materials for the development of novel solid-state functions.

Key words supramolecular chemistry, host-guest systems, heterocycles, electron transfer, chalcogen bond, charge-transfer complex, overcrowded ethylene, crystal structure

1 Introduction

Secondary bonding interaction (SBI) has recently attracted a great deal of attention. It is of special importance in the field of crystal engineering,[1,2] which enables the prediction and regulation of crystal packing, thus contributing to the design of new solids with desired physical and chemical properties. Along with the weak hydrogen bond (WHB) which involves less acidic C-H as a hydrogen donor,[3] the chalcogen bond (ChB)[4,5] is a representative SBI that exhibits high directionality in a crystal. In an atomic array of LB ••• E–Z, where E is an electrophilic chalcogen atom and Z is an electron-withdrawing group, a Lewis base (LB) is bound to E through electron donation from n(LB) to the σ*(E–Z) orbital. Electrostatic attraction also plays an important role in ChB. Each atom has two σ-holes, which are positively charged regions that extend in the direction opposite of each E-Z bond. Thus, the strength of the ChB is influenced by several factors, including, the nature of the electron-deficient Z group attached to E, the linearity of the LB ••• E–Z atomic array, and the basicity of LB.[6] The E atom are has dramatic effects because it becomes both more polarizable and electropositive as it grows. Both of these factors lead to a deeper σ-hole, and thus to a generally stronger ChB for Se than for S, as has been demonstrated for a series of compounds.[7] [1,2,5]Chalcogenadiazoles[8] possess both an E atom and imine nitrogen atoms, and thus can form ChB via E ••• N contacts among themselves. They are versatile units for the generation of supramolecular synthons with an $(E \bullet\bullet\bullet N)_2$-square-dyad motif (Z = N, LB = N) with duplicate ChB (Scheme 1a).[9] The nitrogen atom of a cyano group is a much stronger LB than that of an imine group, and the ChB through E ••• N≡C contacts has been reported

for certain inorganic materials.[10] We previously reported that short, linear E ••• N≡C contacts are quite often found in a series of tetracyanoquinodimethane (TCNQ) derivatives fused with chalcogenadiazole(s), which are characterized by the geometrical parameters shown in Scheme 1c, as in the case of WHB (Scheme 1d). In both their pristine crystals and their molecular complexes and anion radical salts,[11] the molecules are connected to each other by ChB with dual E ••• N≡C contacts as shown in Scheme 1b, which induces characteristic features and functions, such as molecular recognition or electrical conduction in the solid state. This Account describes our journey studying a family of chalcogenadiazolo-TCNQs over the decades.

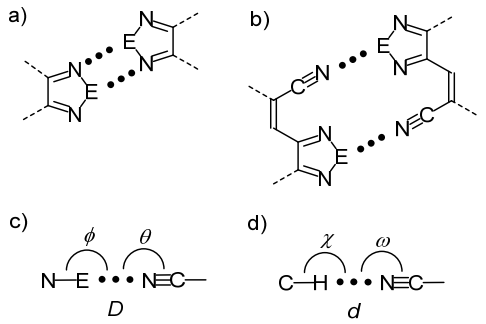

Scheme 1 (a) (E ••• N)$_2$-square-dyad and (b) E ••• N≡C motifs of chalcogen bond (ChB). Geometrical definition of (c) ChB and (d) WHB.

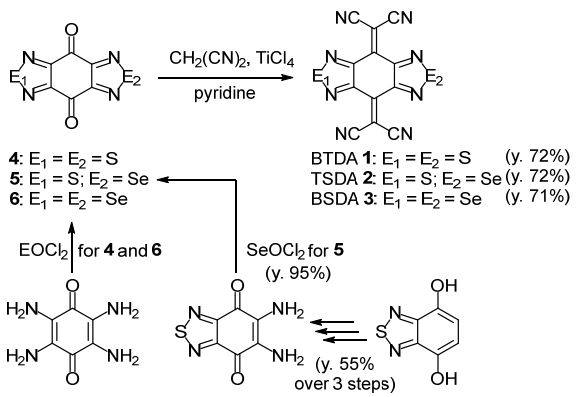

Scheme 2 Preparation of BTDA (**1**), TSDA (**2**), and BSDA (**3**)

2 Bis[1,2,5]thiadiazolo-TCNQ (BTDA)

2.1 Chalcogen Bonds in Crystal Structures of BTDA and its Se-analogues

Bis[1,2,5]thiadiazolotetracyanoquinodimethane (BTDA, **1**)[11,12] is a π-extended analogue of TCNQ that can be prepared from the corresponding quinone **4**[13] by condensation reactions with $CH_2(CN)_2$ in the presence of $TiCl_4$ and pyridine[14,15] (Scheme 2). It undergoes reversible four-stage one-electron reduction at –0.40, –0.87, –1.59, and –2.14 V vs Fc/Fc^+ in MeCN. Based on the comparison of E_1^{red} with that of the parent TCNQ (E_1^{red}: –0.20 V), **1** is a slightly weaker acceptor, as for other TCNQ derivatives annulated with two aromatic heterocycles.[16] Thanks to the π-extension, however, both singly-charged anion radical ($\mathbf{1}^{-\bullet}$) and doubly-charged dianion ($\mathbf{1}^{2-}$) were isolated as stable salts.[17] The triply-charged trianion radical ($\mathbf{1}^{3-\bullet}$) could be generated electrochemically,[18] and an electron spin resonance study showed that it has a large spin density in the heterocyclic part. In contrast to other sterically deformed TCNQ derivatives fused with benzene rings,[19] **1** and its anionic states adopt planar geometries.

As revealed by an X-ray analysis (250 K), a striking feature of its crystal packing is the formation of a coplanar two-dimensional (2D) sheet-like network (Figure 1), in which a molecule of **1** is surrounded by four neighbors connected by eight-fold S ••• N≡C contacts.[11,20,21] The E ••• N contact distance [*D*: 3.03(1) Å, E = S] is much smaller than the sum of the van der Waals (vdW) radii of S and N (3.35 Å). The outstanding linearity of the N-S ••• N≡C atomic array is shown by the angles of N-E ••• N (ϕ) and E ••• N≡C (θ) [167.9(1)° and 170.7(1)°, respectively, E = S] (Scheme 1c). The laterally expanded 2D sheet-like networks are regularly stacked at the heterocyclic parts with an equal interplanar distance of 3.56 Å, which is larger than the usual π-π overlap of aromatic rings (3.40 Å). Thus, we conclude that the packing arrangement of **1** is controlled by ChB through S ••• N≡C contacts.

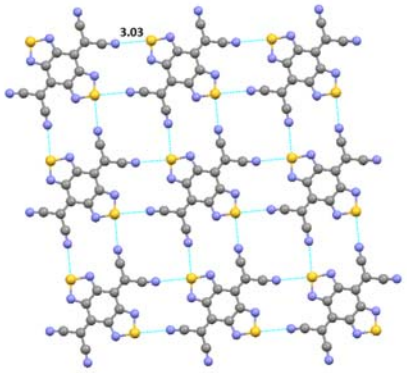

Figure 1 2D sheet-like network in **1** by ChB through S ••• N≡C contacts. The distance is shown in Å.

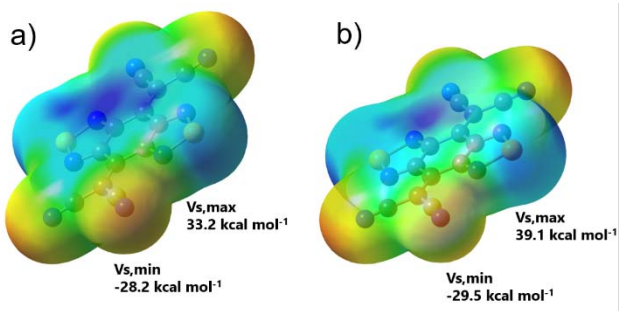

Figure 2 Electrostatic potentials of (a) BTDA **1** and (b) BSDA **3** calculated by DFT method (M06-2X/6-31G**) based on the crystallographic coordinates.

Its Se-analogues (TSDA, **2** and BSDA, **3**),[11,22] in which one or two thiadiazole rings are replaced by selenadiazole rings, were prepared from the corresponding quinones **5**[11] and **6**,[13] as shown in Scheme 2. They adopt crystal packing isomorphous to **1**, with complete positional disorder of S and Se in **2**. The strongest ChB is suggested through the shorter Se ••• N≡C contacts in **3** [*D*: 2.94(1) Å (sum of vdW radii of Se and N: 3.45 Å), ϕ: 169.6(1)°, θ:

169.2(1)°measured at 250 K]. According to DFT calculations (M06-2X/6-31G**) for **1** and **3**,[21] **3** has deeper σ-holes than in **1**, as shown by the greater $V_{s,max}$ value (+33.2 kcal mol^{-1} for **1** and +39.1 kcal mol^{-1} for **3**, respectively) in their electrostatic potential maps (Figure 2). Thus stronger electrostatic attraction is expected by the Se ••• N≡C contact. Natural bond orbital analyses showed that the E ••• N≡C contact induces the donation of a lone pair of the cyano nitrogen to the antibonding E-N orbital, with a second-order perturbation stabilization of +2.05 kcal mol^{-1} for **1** and +4.84 kcal mol^{-1} for **3**, respectively.

The above X-ray analyses and DFT calculations demonstrate that bis[1,2,5]chalcogenadiazolo-TCNQs are unique electron acceptors endowed with the ability to form ChB through E ••• N≡C contacts. Despite the strong ChB in Se-analogues, further studies on the exploitation of ChB-related functions have been mainly conducted using **1**, based on the higher solubility and stronger electron-accepting properties of **1** than of **2** and **3** (E_1^{red}: –0.50 V and –0.63 V vs Fc/Fc$^+$ in MeCN, respectively).

2.2 Electronic Effects of Chalcogen Bonds in Organic Conductors of BTDA

The theoretical consideration indicated that the LUMO of BTDA (**1**) has the same symmetry as that of TCNQ. While there are large coefficients on cyano groups, S atoms are on the nodal plane, suggesting that stronger ChB through S ••• N≡C contact is expected for anion-radical salts due to an increase in the negative charge-density on cyano N atoms, whereas σ-holes on S atoms are not affected by one-electron reduction. Due to its adequate electron-accepting ability, **1** was readily reduced to **1**$^{-\bullet}$ upon treatment with 1.5 equivalents of iodide, such as EtMe$_3$N$^+$I$^-$, to give a stable crystalline salt of EtMe$_3$N$^+$**1**$^{-\bullet}$.[23] The X-ray analysis revealed the formation of a coplanar ribbon-like network by ChB though S ••• N≡C contacts (Figure 3a), which is

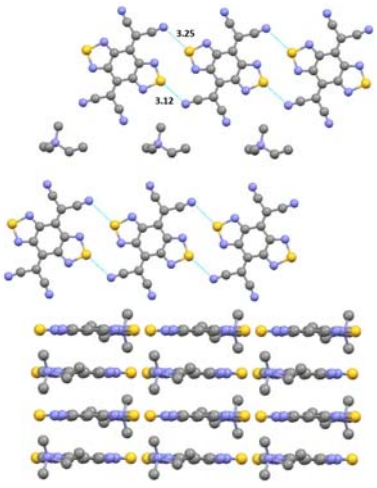

Figure 3 Molecular packing in the crystal of EtMe$_3$N$^+$**1**$^{-\bullet}$ (1:1) salt. The distances corresponding to D_1 and D_2 are shown in Å. (a) Top view showing the ribbon network and (b) side view showing π-π stacking. The geometrical data are as follows: D_1: 3.12 Å, ϕ_1: 149.3°, θ_1: 120.2°; D_2: 3.25 Å, ϕ_2: 150.1°, θ_2: 115.7°, respectively, for two sets of S ••• N≡C contacts

just a strip-subunit of a 2D sheet-like network of pristine **1**. The counter cations are incorporated between the two laterally expanded ribbon networks. The N$^+$ atom is located on the same plane as **1**$^{-\bullet}$, which maximizes the Coulombic attraction between **1**$^{-\bullet}$ and the counter cation. Perpendicular to the ribbon network, a columnar π-π stack of **1**$^{-\bullet}$ is formed with a short interplanar distance of 3.24 Å (Figure 3b), which would result from the orbital interaction with formation of the band structure. This salt exhibits a high electrical conductivity in the direction of π-π stacking (0.030 S cm^{-1}), despite the completely filled conduction band of the salt with a cation : **1**$^{-\bullet}$ molar ratio of 1 : 1 (Mott insulator). This means that the disproportionation [**1**$^{-\bullet}$ (mol-1) + **1**$^{-\bullet}$ (mol-2) ⇌ **1**^{0} (mol-1) + **1**$^{2-}$ (mol-2); mol-1 and -2 are the neighboring molecules in the columnar stack] in the columnar stack is facilitated by the reduced on-site Coulombic repulsion in the doubly charged species due to the enlarged π-system of **1** compared to those of other TCNQ-type electron acceptors.

The anion radical salts are sometimes formed with a molar ratio other than 1:1 (e.g. 2 : 3, 1 : 2, or 2 : 5), and higher conductivities are expected for such salts of **1**$^{-\bullet}$ since they have a partially filled conduction band. In those salts, the electron conduction can be induced by the formal electron exchange [**1**$^{-\bullet}$ (mol-1) + **1**^{0} (mol-2) ⇌ **1**^{0} (mol-1) + **1**$^{-\bullet}$ (mol-2)]. Although such regulation of the molar ratio is usually difficult, it is easy for a series of salts of **1**$^{-\bullet}$ with alkylammoniums as a counter cation, by the crystal-engineering approach based on ChB through S ••• N≡C contacts. Thus, further X-ray analyses showed that above-mentioned ribbon-like networks were commonly observed in the crystals of two other salts [Et$_4$N$^+$**1**$_2^{-\bullet}$ (1:2) and *n*Bu$_3$MeN$^+$**1**$_2^{-\bullet}$ (1:2)]. . Again, the counter cations are incorporated between the ribbon networks. Accordingly, for the combination of **1**$^{-\bullet}$ with the larger ammonium, the π-π stacking of **1**$^{-\bullet}$ could not be maintained while maintaining a molar ratio of 1 : 1. Thus, the ratio gradually changes to 2:3, 1:2, and then 2:5, with formal insertion of neutral **1** between the molecules of **1**$^{-\bullet}$ in the columnar stack, upon elongation of the side chain of the alkylammonium. In this way, small ammoniums such as H$_4$N$^+$, Me$_4$N$^+$ only formed 1:1 salts along with EtMe$_3$N$^+$, whereas Et$_2$Me$_2$N$^+$ and Et$_4$N$^+$ only formed 2:3 and 1:2 salts, respectively. For the combination with a larger R$_4$N$^+$, only 1:2 salts were obtained for *n*Pr$_4$N$^+$ and *n*Bu$_4$N$^+$ whereas *n*Pen$_4$N$^+$ gave only 2:5 salt. These salts with a partially-filled conduction band are generally highly conductive [e.g., 0.32 S cm^{-1} measured on a compaction pellet for *n*Bu$_4$N$^+$**1**$_2^{-\bullet}$ (1:2)]. Thus, modification of the molar ratio by ChB-based crystal engineering can be used to control the electron conduction of **1**$^{-\bullet}$ salts.

It would be particularly interesting to clarify whether or not electron conduction can be induced along the ribbon network formed by ChB. Measurements performed on a single-crystalline sample of *n*Bu$_3$MeN$^+$**1**$_2^{-\bullet}$ (1:2) showed that conductivity was observed not only in the direction of π-π stacking (0.59 S cm^{-1}) but also along the ribbon network expanded laterally (0.027 S cm^{-1}), demonstrating the 2D electronic structure of the **1**$^{-\bullet}$ salts.[23] The direction passing over the counter cation showed a resistivity 100-fold greater than that in the stacking direction. This example clearly shows that electron conduction occurs along the molecular network formed by ChB, which plays an important role in modification of the solid-state electronic structure.[24]

Both anion radicals salt and certain solid-state charge-transfer (CT) complexes of **1**,[25] such as tetraceno[5,6-cd:11,12-c'd']bis[1,2]diselenole (tetraselenatetracene, TSeT) complex, exhibit high electrical conductivity. The crystal of TSeT•**1** (1:1) complex is a molecular metal with partial charge-transfer of 90%, the conductivity of which increases with a decrease in temperature. X-ray structural analysis revealed the formation of segregated columnar stacks for both TSeT and **1** (interplanar distance: 3.32 Å and 3.26 Å, respectively), which are the major conduction paths in the solid. Between the columnar stacks, there are close contacts between Se atoms of TSeT and cyano groups of **1** (Figure 4a). These ChB contacts were shown to be the key factor in stabilizing the metallic state, with suppression of the metal-insulator transition (Peierls transition) even at very low temperature down to 1.5 K.[26]

The absence of S ••• N≡C contact in the crystal of TSeT•**1** can be rationalized by considering that the stronger ChB involving Se atom overwhelms the ChB through S ••• N≡C contacts among **1**. In other CT complexes of **1** with electron donors that lack Se atoms, the molecules of **1** are connected by S ••• N≡C contacts. In the semiconducting CT complex with tetrathiafulvalene (TTF)[27] with a partial charge-transfer of 6%, a TTF molecule is incorporated in the cavity formed by ChB through S ••• N≡C contacts, showing that clathrate-type inclusion occurs in CT complexes of **1** with weaker electron donors[28] (Figure 4b).

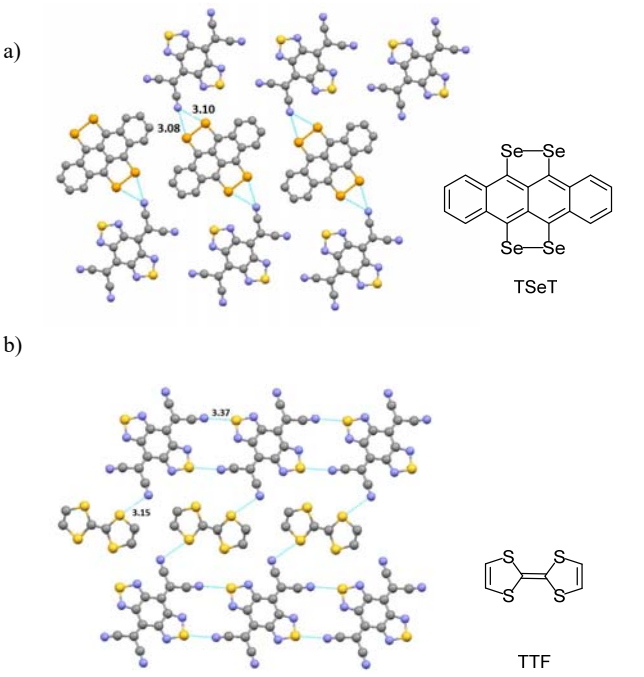

Figure 4 (a) Molecular packing in the crystal of TSeT•**1** (1:1) CT complex viewed along the segregating stacks. The distances corresponding to D_1 and D_2 are shown in Å. The geometrical data are as follows: D_1: 3.08 Å; θ_1: 164.7°; D_2: 3.10 Å; θ_2: 124.2°, respectively, for two sets of Se ••• N≡C contacts, and the separation of 3.87 Å for S ••• N≡C is too far to be considered as ChB. (b) Molecular packing in the crystal of TTF•**1** (1:1) CT complex viewed along the mixed stack. The distances corresponding to D_1 and D_2 are shown in Å. The geometrical data are as follows: D_1: 3.37 Å, ϕ_1: 125.7°, θ_1: 134.1°; D_2: 3.15 Å; θ_2: 104.0°, respectively, for two sets of S ••• N≡C contacts.

2.3 Molecular Recognition by Chalcogen Bonds in Molecular Complexes of BTDA

Molecular recognition properties of BTDA (**1**) upon the formation of clathrate complexes[11] by ChB through S ••• N≡C contacts were first demonstrated when finely ground yellow crystals of **1** were suspended in a liquid containing a mixture of *o*-, *m*-, and *p*-xylene to give CT complex, as a red powder, which selectively includes *p*-xylene. The co-presence of ethylbenzene did not affect the selectivity. Heating of the resulting solid liberated pure *p*-xylene accompanied by the regeneration of **1**, demonstrating that clathrate formation of **1** can be used to separate *p*-xylene from its isomer mixture (Scheme 3).

X-ray analysis of *p*-xylene•**1** (1:1) revealed that, perpendicular to an alternating donor-acceptor columnar stack, a ribbon-network of **1** is formed by ChB through S ••• N≡C contacts (D_1: 3.22 Å, ϕ_1: 137.2°, θ_1: 112.2°; D_2: 3.24 Å, ϕ_2: 142.8°, θ_2: 111.1°, respectively, for two sets of S ••• N≡C contacts). An inclusion cavities that incorporate *p*-xylene molecules is formed between the two ribbon networks, as similar to Figure 4b. Molecular recognition is the result of molecular shapes of *o*- and *m*-xylene that are unsuitable for inclusion in the cavity formed by ChB. Recrystallization of **1** from pure *o*- and *m*-xylene resulted in no formation of CT complexes, which demonstrates the remarkable recognition properties of **1** via ChB.

Selective complexation of **1** also occurs for *p*-chlorotoluene among its isomers (E^{ox}: +1.74 - +1.87 V vs Fc/Fc^+ in MeCN), similar to the results with xylene (+1.57 - +1.69 V). On the other hand, not only *p*- but also *o*-isomers of chloroanisoles (+1.38 - +1.48 V) form stable CT complexes with **1**. For a series of methylanisoles (+1.15 - +1.23 V), all of the isomers gave crystalline CT complexes with **1**. By considering that *p*-methylanisole•**1** (1:1) and *o*-methylanisole•**1** (1:1) have a similar crystal packing with ribbon networks via ChB through S ••• N≡C contacts (Figure 5), the enhanced CT interaction in the donor-acceptor mixed columnar stack covers up the unsuitable molecular shape of *o*-isomer to be located in the inclusion cavity, thus concealing the recognition properties upon clathrate formation when the CT interaction between **1** and the donor increases.

With the use of a weaker electron acceptor **2** instead of **1**, CT interaction decreases. Thus, selectivity for *p*-isomers was apparent for chloroanisoles and methylanisoles. On the other hand, while the much weaker acceptor **3** does not form any crystalline complexes with the disubstituted benzenes shown above, it does form such complexes with dimethoxybenzene isomers with much lower E^{ox} values (+0.86 - +1.05 V). It was shown that molecular recognition of **1** – **3** via ChB through E ••• N≡C contacts can be realized with the proper combination of electron donors to attain suitable CT interaction, because the selectivity is concealed for the donors that are too strong, whereas donors that are too weak do not form CT-type clathrates with **1** - **3**. Thus, while a complementary shape and size are important, in general, for host-guest-type complexation, the present clathrates are also stabilized by CT interaction, resulting in recognition not only by the shape but also by the electron-donating properties of the guest.

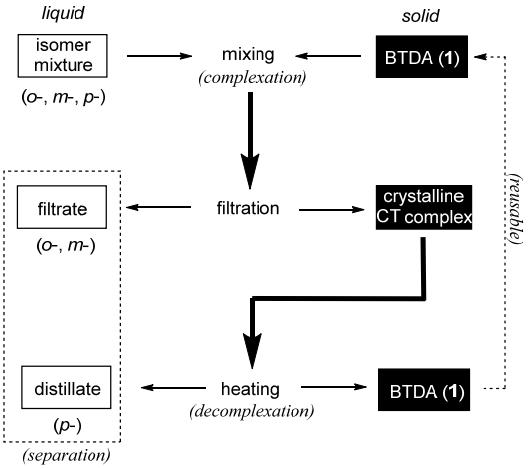

Scheme 3 Simple mixing-filtration-heating process for separation of *p*-xylene from the isomer mixture by using clathrate formation of BTDA (**1**) by ChB through S ••• N≡C contacts

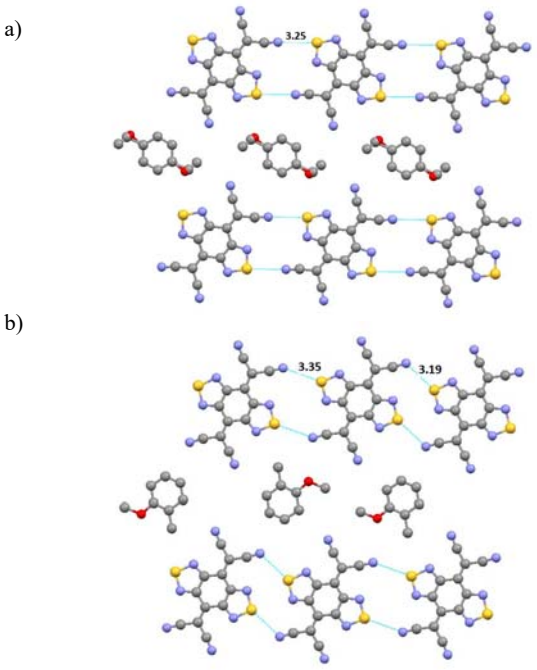

Figure 5 (a) Molecular packing in the crystal of *p*-methylanisole•**1** (1:1) CT complex viewed along the mixed stack. The distance corresponding to *D* is shown in Å. The geometrical data are as follows: *D*: 3.25 Å, ϕ: 169.3°, θ: 174.7° for the S ••• N≡C contact. The methyl and methoxy groups are positionally disordered. (b) Molecular packing in the crystal of *o*-methylanisole •**1** (1:1) CT complex viewed along the mixed stack. The distances corresponding to D_1 and D_2 are shown in Å. The geometrical data are as follows: D_1: 3.18 Å, ϕ_1: 147.0°, θ_1: 120.8°; D_2: 3.35 Å, ϕ_2: 137.0°, θ_2: 146.5°, respectively, for two sets of S ••• N≡C contacts.

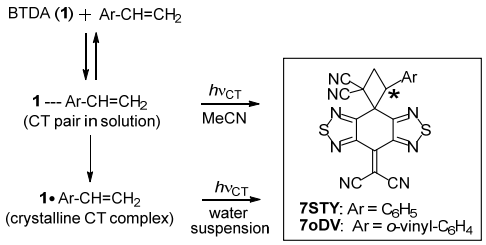

Scheme 4 Cycloaddition of BTDA (**1**) with aryl olefins under CT excitation conditions

2.4 Single-crystalline-state Photoreaction of Molecular Complexes of BTDA

When BTDA (**1**) and aryl olefins, such as styrene (STY) or *o*-divinylbenzenes (oDV), were mixed in MeCN, new absorption bands extending to 550 nm were observed, which correspond to the formation of CT pairs in solution. When the CT pairs were photoirradiated at their CT absorption bands, **1** and aryl olefins first converted to the radical-ion pairs that underwent regioselective [2+2]-type cycloaddition to give adducts (**7STY** and **7oDV**) (Scheme 4). Due to the small association constant (0.85 and 1.1 M^{-1} for **1** - - STY and **1** - - oDV, respectively, in MeCN at 295 K), cycloaddition was sluggish in solution. More efficient cycloaddition occurred when the CT excitation reactions were conducted for a water suspension of crystalline CT complex of STY•**1** (1:1) or oDV•**1** (1:1) to give the same product in a high isolated yield (e.g., 91% for **7oDV**); these are the first examples of photoinduced electron-transfer reactions conducted in the solid state.[29]

X-ray analysis of oDV•**1** (1:1) crystal showed that it adopts molecular packing with ribbon networks formed via ChB through S ••• N≡C contacts (Figure 6a), which is quite similar to the results with methylanisole complexes, showing that the inclusion cavity formed by ChB in **1** provides a suitable reaction environment for oDV to undergo smooth cycloaddition with **1**.

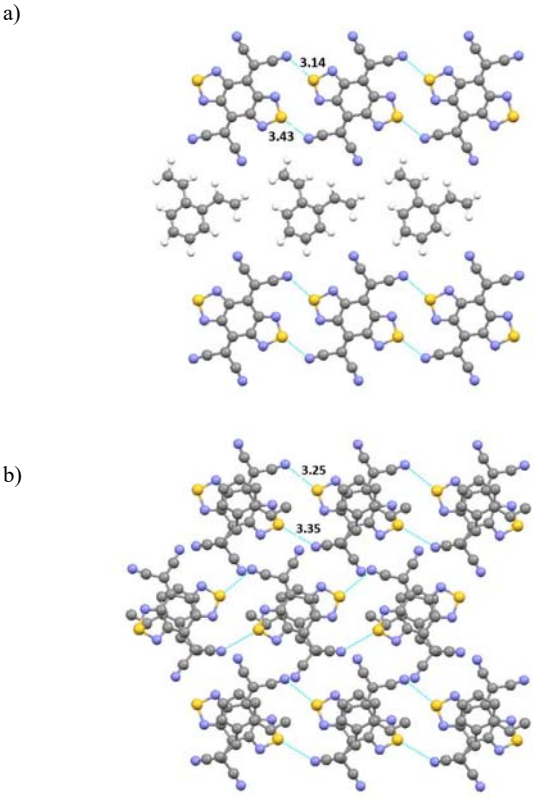

Figure 6 Molecular packing in the crystal of *o*-DV •**1** (1:1) CT complex viewed along the mixed stack (a) before and (b) after the single-crystal-to-single-crystal photoinduced electron-transfer reaction. The distances corresponding to D_1 and D_2 are shown in Å. The geometrical data are as follows: (a) D_1: 3.14 Å, ϕ_1: 142.6°, θ_1: 114.8°; D_2: 3.43 Å, ϕ_2: 134.7°, θ_2: 106.3°, respectively, for two sets of S ••• N≡C contacts; (b) D_1: 3.35 Å, ϕ_1: 137.7°, θ_1: 117.6°; D_2: 3.25 Å, ϕ_2: 145.7°, θ_2: 117.0°, respectively, for two sets of S ••• N≡C contacts.

Actually, oDV•**1** (1:1) is transformed into **7oDV** while maintaining its single crystallinity,[30] so that the solid-state photoinduced electron-transfer reaction could be followed by X-ray analyses. The crystal structure of the as-photolyzed **7oDV** is quite similar to that of oDV•**1** (1:1) and exhibits ribbon networks with S ••• N≡C contacts (Figure 6b), showing that ChB can facilitate the single-crystal-to-single-crystal transformation upon topotactic transformation.

Based on the fact that achiral components of **1** and oDV crystallized in a chiral space group[31] ($P2_1$), the molecular arrangement in the reacting face-to-face overlap is chiral. Although such chirality is lost upon dissolution, photoconversion resulted in a transformation of chirality of crystal packing to point chirality of the product molecule. When a certain single crystal of oDV•**1** (1:1) (right-handed crystal) was photoirradiated, (*R*)-(+)-**7oDV** was obtained in 96% ee, whereas (*S*)-(-)-**7oDV** with 95% ee was obtained upon irradiation of another single crystal (left-handed crystal) which has only the mirror-imaged face-to-face overlap (Scheme 5). This photoreaction demonstrates successful absolute asymmetric synthesis,[32] in which no external chiral element is used to generate optically pure material.

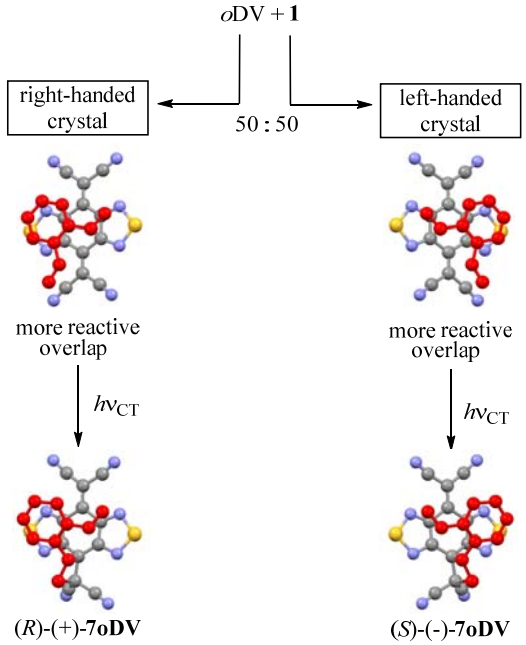

Scheme 5 Absolute asymmetric synthesis of **7oDV** via single-crystalline state photoinduced electron transfer reaction of oDV•**1** (1:1)

2.5 Overcrowded Ethylene Composed of a BTDA Substructure

BTDA-dimer (**10**)[33] is a π-extended analogue with a tetracyanobiphenoquinodimethane skeleton[34] fused with four thiadiazole rings. In contrast to **1** with a planar geometry, the sterically hindered bis(tricyclic ene) structure endows **10** with unique properties as an overcrowded ethylene,[35] similar to bianthrone **11**[36] which is known to be a representative thermochromic and mechanochromic material (Scheme 6). A color change of **11** upon partial isomerization from a yellow stable form with a folded geometry into a green metastable form with a twisted geometry has been postulated. However, the identity and geometrical parameters of the metastable form of **11** were not clarified for a long time since the metastable form could not be isolated until very recently by the introduction of proper substituents.[37] In contrast, the yellow folded form and violet twisted form of **10** were easily isolated and analyzed by X-ray to confirm their geometrical features, thanks to ChB through S ••• N≡C contacts.

Upon treatment of $(Na^+)_2\mathbf{1}^{2-}$ salt with aqueous HCl, a dihydro derivative of BTDA (**12**) was obtained,[17] which was further converted to mono(dicyanomethylene) derivative (**13**)[11] (Scheme 7). Dehydrogenative dimerization using SeO_2 gave **10**. A solution in $ClCH_2CH_2Cl$ exhibits a violet color characteristic of the twisted form while exhibiting reversible four-stage one-electron reduction (−0.30, −0.47, −1.48, and −1.63 V vs Fc/Fc^+ in CH_2Cl_2). From this solution, yellow crystals were obtained upon concentration. Crushing of these yellow crystals gave a violet color (mechanochromism), whereas a yellow color returned when the crushed violet solid was heated (thermochromism). This behavior is characteristic of an overcrowded ethylene. According to DFT calculations (M06-2X/6-31G**), the folded conformer in the gas phase is marginally more stable than the twisted form only by 2.47 kcal mol^{-1}.

In the crystal of the yellow folded form of **10**, a 2D sheet-like network is formed by ChB through S ••• N≡C contacts (Figure 7a), which stabilizes the folded form in the pristine crystal. The observed network is similar to those in **1** and **13**. For the latter, ChB through S ••• N≡C contacts were observed as well as a (S ••• $N)_2$-square-dyad motif (Figure 8). On the other hand, the violet twisted form of **10** was isolated as a solvate upon recrystallization from CH_2Cl_2 or PhCN. X-ray analysis of the latter showed that the ChB network between **10** is partially broken into a 1D network to incorporate solvent molecules (Figure 7b). This is the first demonstration that a change in intermolecular interactions in a crystal allows the isolation of multiple forms of overcrowded ethylenes.[38]

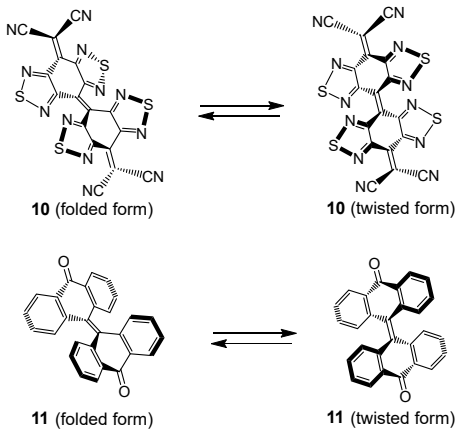

Scheme 6 BTDA-dimer-type overcrowded ethylene (**10**) and bianthrone (**11**)

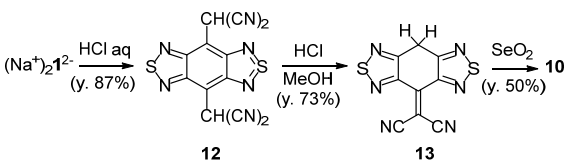

Scheme 7 Preparation of BTDA-dimer (**10**)

a)

b)

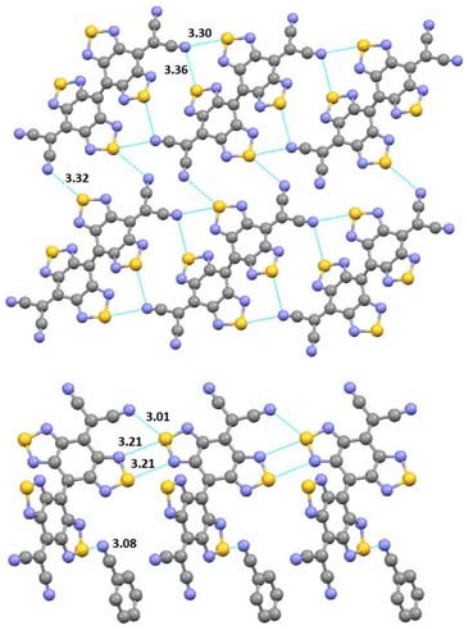

Figure 7 Molecular packing of BTDA-dimer (**10**) in the crystals of (a) the folded conformer and (b) the twisted conformer containing benzonitrile (solvate). The distances corresponding to $D_1 - D_4$ are shown in Å. The geometrical data are as follows: (a) D_1: 3.30 Å, ϕ_1: 164.4°, θ_1: 165.3°; D_2: 3.32 Å, ϕ_2: 131.8°, θ_2: 108.7°; D_3: 3.36 Å, ϕ_3: 126.2°, θ_3: 95.3°, respectively, for three sets of S ••• N≡C contacts; (b) D_1: 3.01 Å, ϕ_1: 150.3°, θ_1: 114.6°; D_2: 3.08 Å, ϕ_2: 166.8°, θ_2: 119.2°, respectively, for two sets of S ••• N≡C contacts, and D_3: 3.21 Å, ϕ_3: 173.9°; D_4: 3.21 Å, ϕ_4: 171.6°, respectively, for (S ••• N)$_2$ -square-dyad motif.

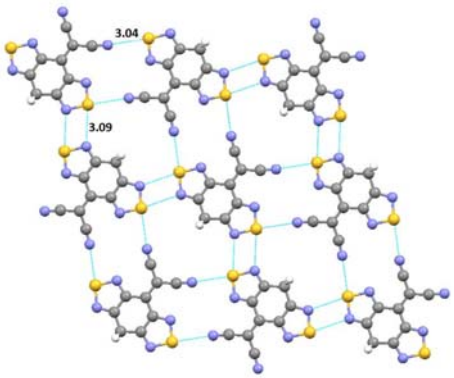

Figure 8 2D sheet-like network in **13**. The distances corresponding to D_1 and D_2 are shown in Å. The geometrical data are as follows: D_1: 3.04 Å, ϕ_1: 174.5°, θ_1: 174.6° for the S ••• N≡C contact, and D_2: 3.09 Å, ϕ_2: 171.8° for (S ••• N)$_2$-square-dyad motif.

3 TCNQ Analogues Fused with a [1,2,5]Chalcogenadiazole

3.1 Crystal Structures of Chalcogenadiazolo-TCNQs

Tetracyanoquinodimethanes fused to only one chalcogenadiazole (**14** - **16**)[39] were prepared from the corresponding dihalobenzochalcogenadiazoles[9g] by using Pd(0)-catalyzed coupling with NaCH(CN)$_2$ (Scheme 8). These are strong electron acceptors (E_1^{red}: –0.16, –0.26, and –0.34 V vs Fc/Fc$^+$ in MeCN for **14** - **16**, respectively) and form highly conductive CT complexes with some derivatives of TTF.

After we examined a series of crystal structures of BTDA (**1**) with ChB, which induces various functions in the solid state, we unexpectedly found that the crystal of thiadiazolo-TCNQ (**15**) does not exhibit ChB through S ••• N≡C contacts. The molecular arrangement is similar to that of oxadiazolo-TCNQ (**14**). Thus, the crystal structure is characterized by the coplanar dimeric structure (Figure 9a,b), which is connected by WHB through C-H ••• N≡C contacts (Scheme 1d). Such observations of the WHB-dyad can be rationalized by supposing that ChB is overwhelmed by WHB in **15**, especially because of the enhanced acidity of a C-H group on the quinoid sp2 carbon due to polarization.

On the other hand, the dimeric structure caused by WHB is present in selenadiazolo-TCNQ (**16**). However, molecules are further connected by ChB through Se ••• N≡C contact as well as (Se ••• N)$_2$-square-dyad motif to form another dimeric structure by ChB (ChB-dyad) (Figure 9c). By connecting another ChB through Se ••• N≡C contact (D: 3.02 Å, ϕ: 169.2°, θ: 152.4°), there is a 2D sheet-like network in **16**. Thus, the stronger ChB involving a Se atom can help determine the crystal packing along with WHB.

Cooperative control of crystal packing by ChB and WHB occurred not only for Se-containing compounds, as shown by a TCNQ derivative (**17**)[40] that fused with both thiadiazole and pyrazine ring by weakening the C-H-donating properties for WHB more than in the case of **15**. Thus, **17** adopts a planar geometry and forms coplanar 2D sheet-like network, as in **1**, with the formation of both a ChB-dyad and a WHB-dyad (Figure 10).

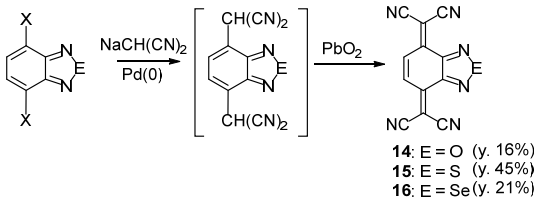

Scheme 8 Preparation of chalcogenadiazolo-TCNQs (**14** - **16**)

a)

b)

c)

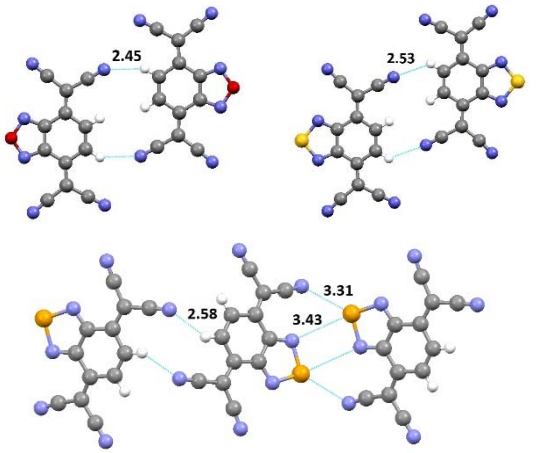

Figure 9 WHB-dyad formation in chalcogenadiazolo-TCNQs (**14** - **16**). The distances corresponding to d, D_1 and D_2 are shown in Å. The geometrical data are as follows: (a) **14**: d: 2.44 Å, χ: 150°, ω: 152°; (b) **15**: d: 2.53 Å, χ: 129°, ω: 169°; (c) **16**: d: 2.58 Å, χ: 147°, ω: 124°, respectively, for each C-H ••• N≡C contact; D_1: 3.31 Å, ϕ_1: 137.2°, θ_1: 104.4° for the S ••• N≡C contact; and D_2: 3.43 Å, ϕ_2: 154.7° for (S ••• N)$_2$-square-dyad motif.

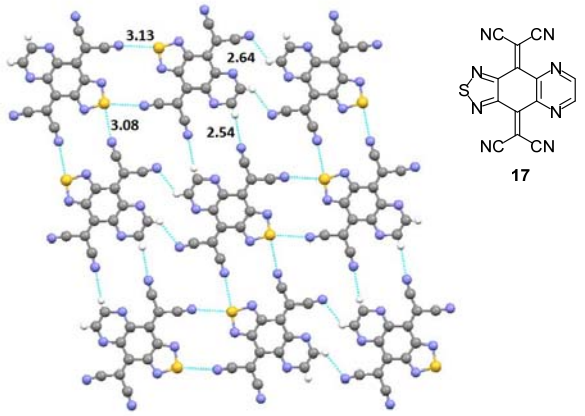

Figure 10 2D sheet-like network in **17**. The distances corresponding to D_1, D_2, d_1, and d_2 are shown in Å. The geometrical data are as follows: D_1: 3.08 Å, ϕ_1: 171.6°, θ_1: 171.6°; D_2: 3.13 Å, ϕ_2: 157.4°, θ_2: 166.1°, respectively, for two sets of S ••• N≡C contacts, and d_1: 2.54 Å, χ_1: 127°, ω_1: 112°; d_2: 2.64 Å, χ_2: 173°, ω_2: 177°, respectively, for two sets of C-H ••• N≡C contacts.

3.2 Crystal Structures of Chalcogenadiazolo-TCNNQs: E ••• N≡C Chalcogen Bond versus C-H ••• N≡C Weak Hydrogen Bond

The crystal structures shown in the previous subsection indicate that ChB through E ••• N≡C contacts and WHB through C-H ••• N≡C contacts act cooperatively to determine the crystal packing, as found in selenadiazolo-TCNQ (**16**) and in pyrazine-fused derivative (**17**) with 2D sheet-like networks. On the other hand, WHB predominantly determines the molecular arrangement with overwhelming ChB as in the crystal of **15**, suggesting that ChB and WHB could compete against each other. Based on the fact that molecular recognition by ChB[41] is still considered to be in its infancy,[4e] further studies will be needed on tetracyanonaphthoquinodimethane (TCNNQ) derivatives with a non-planar structure, which may accommodate guest molecules more selectively when clathrate-type complexation occurs by ChB through E ••• N≡C contacts. Special attention has been focused on the relative importance of ChB and WHB in determining the crystal packing, and on conditions under which WHB does not interfere with, but rather cooperate with, the molecular recognition via ChB.

Thiadiazole-fused TCNNQs (**18a** – **18c**) and their Se-analogues (**19a** – **19c**) were obtained from the corresponding quinone derivatives (Scheme 9).[12,42] Regardless of the kind of fused ring, namely, benzene (**a**), *o*-xylene (**b**), or naphthalene (**c**), they all adopt a non-planar geometry due to steric repulsion between the cyano groups and the C-H groups at *peri*-positions. X-ray analyses were conducted to examine whether the ChB-based dyad or the WHB-based dyad is formed in **18a** – **18c** and **19a** – **19c** to better understand the relative importance of ChB versus WHB in these systems (Scheme 10).

Thiadiazolo-TCNNQ (**18a**) showed a WHB-dyad (Figure 11a), and ChB through S ••• N≡C contacts are largely suppressed. On the other hand, the corresponding Se-analogue (**19a**) showed only a ChB-dyad through Se ••• N≡C contacts (Figure 11b). This dyad is further connected by ChB and WHB to form a 2D sheet-like network, as detailed later. When the quinodimethane skeleton is fused with an *o*-xylene ring or a naphthalene ring in place of the benzene ring, quite similar ChB dyads were found in crystals of **19b** and **19c**, showing that ChB through Se••• N≡C contacts is a determining factor for a series of selenadiazolo-TCNNQs (**19**) (Scheme 11).

In contrast to the 2D sheet-like network formed through ChB and WHB in **19a** and **19b**, WHB in naphthalene-fused derivative **19c** is less important. The weaker WHB in **19c** is the reason for the adoption of a similar ChB-dyad in S-congener **18c** through S ••• N≡C contacts. The above comparisons can suggest that the balance of the relative importance between ChB and WHB can be adjusted by proper molecular design, and ChB through Se ••• N≡C contacts is robust enough even in the presence of WHB. It is highly likely that ChB and WHB can cooperate to achieve superior recognition properties upon clathrate formation using **19a**.

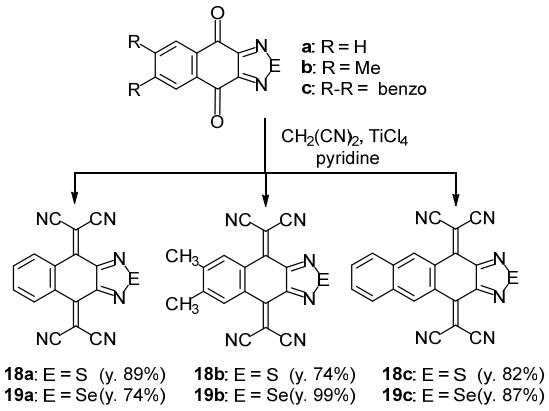

Scheme 9 Preparation of chalcogenadiazolo-TCNNQs (**18a** - **18c** and **19a** - **19c**)

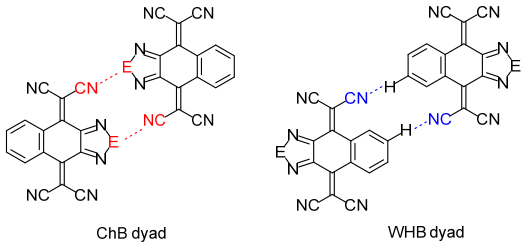

Scheme 10 Two kinds of dyads for chalcogenadiazolo-TCNNQs by SBI

	a: R = H	**b**: R = CH_3	**c**: R-R = benzo
18: E = S	**WHB dyad** **WHB network**	**WHB network**	**ChB dyad** **ChB/π–π network**
19: E = Se	**ChB dyad** **ChB/WHB network**	**ChB dyad** **ChB/WHB network**	**ChB dyad** **ChB/π–π network**

Scheme 11 Classification of crystal structures by SBI-dyad

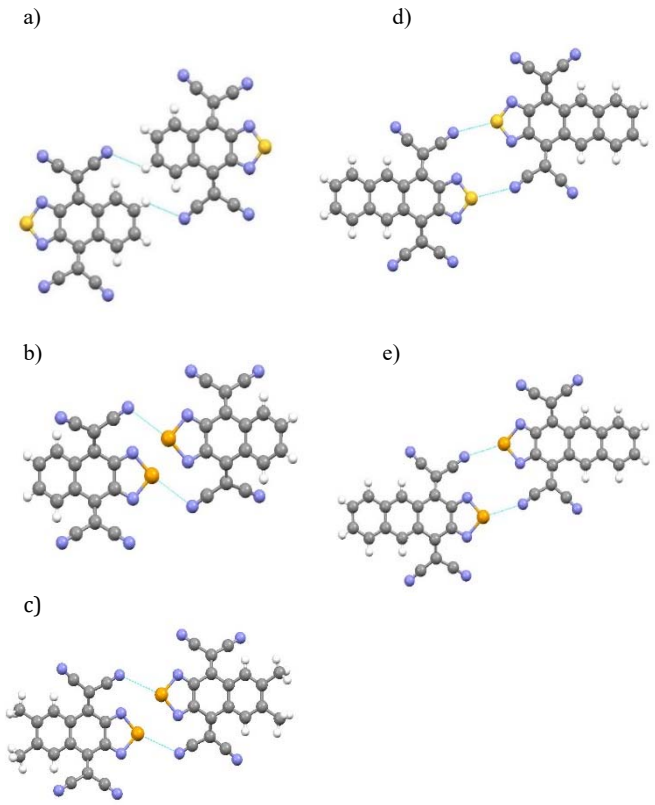

Figure 11 (a) WHB dyad in **18a** and ChB dyad in (b) **19a**, (c) **19b**, (d) **18c**, and (e) **19c**. The geometrical parameters are as follows: (a) *d*: 2.70 Å, χ: 127°, ω: 117°; (b) *D*: 3.16 Å, ϕ: 155.5°, θ: 114.5°; (c) *D*: 3.24 Å, ϕ: 153.4, θ: 123.4°; (d) *D*: 3.14 Å, ϕ: 143.6°, θ: 147.2°; (e) *D*: 3.06 Å, ϕ: 148.6°, θ: 149.3°, respectively.

3.3 Molecular Recognition by Chalcogen Bonds in TCNNQ Derivatives

Upon recrystallization of the yellow solid of selenadiazolo-TCNNQ (**19a**) in the presence of 2,6-dimethylnaphthalene (DMN), red crystals of 2,6-DMN•(**19a**)$_2$ CT complex were obtained.[43] On the other hand, 2,7-DMN did not form the corresponding CT complex with **19a**, despite the fact that 2,6-DMN and 2,7-DMN have very similar molecular shapes to form a eutectic mixture.

Since 2,6-DMN is an important material for industrial applications,[44] the observed ability of **19a** to recognize DMN isomers is outstanding.[45] By a simple mixing-filtration-heating process similar to that shown in Scheme 3, pure 2,6-DMN (97.2 wt%) was obtained with very slight contamination by 2,7-DMN (1.1 wt%) by starting from a C_{12} liquid containing 9.7 wt% of 2,6-DMN and 9.4 wt% of 2,7-DMN. Similar experiments using the S-congener **18a** gave unfruitful results. Even when we used BTDA (**1**) with high recognition properties toward *p*-xylene, pure 2,6-DMN was not obtained (hydrocarbon obtained by thermal decomposition of CT crystals: 2,6-DMN, 77.9 wt%; 2,7-DMN, 4.5%; others, 17. 6 wt%).

To better understand the higher recognition properties of **19a** toward DMN, the crystal packings of pristine **19a** and 2,6-DMN•(**19a**)$_2$ were analyzed in detail. In the crystal of **19a**, the aforementioned ChB-dyad is connected by another ChB (along the crystallographic b axis) to form a 1D dyad-ribbon network, which is further connected by WHB (along the c axis) into a 2D sheet-like network (Figure 12a). In the crystal of 2,6-DMN•(**19a**)$_2$, a very similar molecular arrangement was observed. Thus, a ChB-dyad is connected by another ChB (along the crystallographic b axis) to form a dyad-ribbon network. The original WHB in pristine **19a** is broken but reconnects at the shifted positions to generate a 2D sheet-like network containing inclusion cavities, in which 2,6-DMN is incorporated (Figure 12b). The 2,6-DMN in the cavity is additionally sandwiched in a π-π stacking manner with two molecules of **19a** in the neighboring 2D sheet-like networks. Such a three-dimensional cavity formed by the sterically demanding non-planar electron acceptor **19a** would be key for the observed outstanding molecular recognition, which also involves WHB.

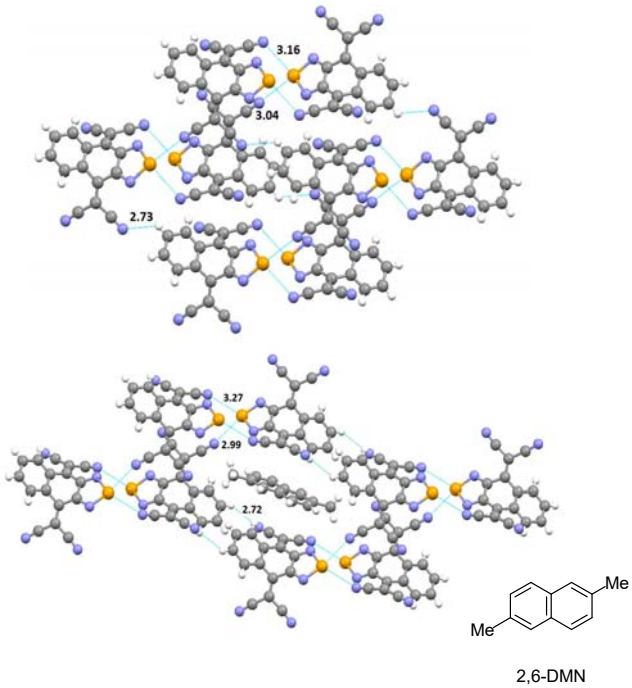

Figure 12 Crystal structures of (a) **19a** and (b) 2,6-DMN•(**19a**)$_2$. The distances corresponding to *D*, D_1, D_2, and *d* are shown in Å. The geometrical parameters are as follows: (a) *D*: 3.04 Å, ϕ: 176.6°, θ: 159.0°; *d*: 2.73 Å, χ: 127°, ω: 128°; (b) D_1: 2.99 Å, ϕ_1: 167.8, θ_1: 159.6°; D_2: 3.27 Å, ϕ_2: 153.8, θ_2: 121.2°; *d*: 2.72 Å, χ: 128°, ω: 146°, respectively.

4 Outlook

As shown above, a family of chalcogenadiazolo-TCNQs that can form ChB are promising materials for the development of novel solid-state functions. Outstanding are sorting electron-donating guest molecules upon CT complexation and photoinduced asymmetric reaction. Furthermore, two-dimensional network structure by ChB is key for the novel electric-field-controllable conductance switching of a BTDA-dimer (**10**)[46] and for the mixed-valence semiconducting framework of BTDA (**1**),[47] which have been reported recently. Both the development of new members of the BTDA family[8e,48] and a better understanding of ChB[49] should continue to expand the chemistry of this attractive class of compounds.

Funding Information

This work was supported by Grant-in-Aid from MEXT and JSPS (Nos. JP20H02719 and JP20K21184 to T.Su., and JP21H01912 and JP21H05468 to Y.I.).

Acknowledgment

This work was also supported by the Research Program of "Five-star Alliance" in "NJRC Mater. & Dev." MEXT. Y.I. and T.Sh acknowledge Toyota Riken Scholar, the Foundation for the Promotion of Ion Engineering.

Conflict of Interest

The authors declare no conflict of interest.

References

(1) Dunitz, J. P. *Pure Appl. Chem.* **1991**, *63,* 177.

(2) (a) Huynh, H.-T.; Jeannin, O.; Fourmigué, M. *Chem. Commun.* **2017**, *53*, 8467. (b) Zhang, Y.; Wang, W. *Crystals* **2018**, *8*, 163; (c) Scilabra, P.; Terraneo, G.; Resnati, G. *Acc. Chem. Res.* **2019**, *52*, 1313.

(3) (a) Desiraju, G. R. *Angew. Chem. Int. Ed.* **1995**, *34*, 2311. (b) Nangia, A.; Desiraju, G. R. *Acta Cryst.* **1998**, A54, 934. (c) Metrangolo, P.; Neukirch, H.; Pilati, T.; Resnati, G. *Acc. Chem. Res.* **2005**, *38*, 386. (d) Desiraju, G. R. *J. Am. Chem. Soc.* **2013**, *135*, 9952.

(4) For recent reviews: (a) Lim, J. Y. C.; Beer, P. D. *Chem* **2018**, *4*, 731. (b) De Vleeschouwer, F.; Denayer, M.; Pinter, B.; Geerlings, P.; De Proft, F. *J. Comput. Chem.* **2018**, *39*, 557. (c) Vogel, L.; Wonner, P.; Huber, S. M. *Angew. Chem. Int. Ed.* **2019**, *58*, 1880. (d) Bamberger, J.; Ostler, F.; Mancheño, O. G. *ChemCatChem*. **2019**, *11*, 5198. (e) Biot, N.; Bonifazi, D. *Coord. Chem. Rev.* **2020**, *413*, 213243. (d) Kolb, S.; Oliver, G. A.; Werz, D. B. *Angew. Chem. Int. Ed.* **2020**, *59*, 22306. (f) Frontera, A.; Bauzá, A. Crystals, **2021**, *11*, 1205. (g) Scheiner, S. *CrystEngComm*. **2021**, *23*, 6821. (h) Tiekink, E. R. T. *Coord. Chem. Rev.* **2022**, *457*, 215397. (i) Tiekink, E. R. T. CrystEngComm, **2023**, *25*, 9,

(5) For early studies: a) Werz, D. B.; Gleiter, R.; Rominger, F. *J. Am. Chem. Soc.* **2002**, *124*, 10638. (b) Werz, D. B.; Staeb, T. H.; Benisch, C.; Rausch, B. J.; Rominger, F.; Gleiter, R. *Org. Lett.* **2002**, *4*, 339. (c) Werz, D. B.; Gleiter, R.; Rominger, F. *J. Org. Chem*. **2002**, *67*, 4290. (d) Werz, D. B.; Gleiter, R.; Rominger, F. *J. Org. Chem.* **2004**, *69*, 2945. (e) Cozzolino, A. F.; Vargas-Baca, I.; Mansour, S.; Mahmoudkhani, A. H. *J. Am. Chem. Soc*. **2005**, *127*, 3184. (f) Cozzolino, A. F.; Vargas-Baca, I. *J. Organometal. Chem.* **2007**, *692*, 2654.

(6) (a) Wang, W.; Ji, B.; Zhang, Y. *J. Phys. Chem. A* **2009**, *113*, 8132. (b) Bauzá, A.; Quiñonero, D.; Deyà, P. M.; Frontera, A. *CrystEngComm* **2013**, *15*, 3137. (c) Sánchez-Sanz, G.; Trujillo, C. *J. Phys. Chem. A* **2018**, *122*, 1369.

(7) (a) Alikhani, E.; Fuster, F.; Madebene, B.; Grabowski, S. J. *Phys. Chem. Chem. Phys.* **2014**, *16*, 2430 (b) Del Bene, J. E.; Alkorta, I.; Elguero, J. *Chem. Phys. Lett.* **2019**, *730*, 466. (c) Zhou, B.; Gabbaï, F. P. *Organometallics* **2021**, *40*, 2371. (d) Haberhauer, G.; Gleiter, R. *Angew. Chem. Int. Ed.* **2020**, *59*, 21236.

(8) (a) Lonchakov, A. V.; Raktin, O. A.; Gristsan, N. P.; Zibarev, A. V. *Molecules* **2013**, *18*, 9850. (b) Pushkarevsky, N. A.; Chulanova, E. A.; Shundrin, L. A.; Smolentsev, A. I.; Salnikov, G. E.; Pritchina, E. A.; Genaev, A. M.; Irtegova, I. G.; Bagryanskaya, I. Y.; Konchenko, S. N.; Gritsan, N. P.; Beckmann, J.; Zibarev, A. V. *Chem. Eur. J.* **2019**, *25*, 806. (c) Radiush, E. A.; Pritchina, E. A.; Chulanova, E. A.; Dmitriev, A. A.; Bagryanskaya, I. Y.; Slawin, A. M. Z.; Woollins, J. D.; Gritsan, N. P.; Zibarev, A. V.; Semenov, N. A. *New J. Chem.* **2022**, *46*, 14490. (d) Scheiner, S. P*hys. Chem. Chem. Phys.* **2022**, *24*, 28944. (e) Ishigaki, Y.; Asai, K.; Jacquot de Rouville, H.-P.; Shimajiri, T.; Hu, J.; Heitz, V. ; Suzuki, T. *ChemPlusChem* **2022**, *87*, e202200075. (f) Scheiner, S. *ChemPhysChem* **2023**, e202200936. (g) Chulanova, E. A.; Radiush, E. A.; Semenov, N. A.; Hupf, E.; Irtegova, I. G.; Kosenkova, Y. S.; Bagryanskaya, I. Y.; Shundrin, L. A.; Beckmann, J.; Zibarev, A. V. *ChemPhysChem* **2023**, e202200876.

(9) (a) Tsuzuki, S.; Sato, N. *J. Phys. Chem. B* **2013**, *117*, 6849. (b) Langis-Barsetti, S.; Maris, T.; Wuest, J. D. *J. Org. Chem.* **2017**, *82*, 5034. (c) Riwar, L. -J.; Trapp, N.; Root, K.; Zenobi, R.; Diederich, F. *Angew. Chem. Int. Ed.* **2018**, *57*, 17259. (d) Ams, M. R.; Trapp, N.; Schwab, A.; Milić, J. V.; Diederich, F. *Chem. Eur. J.* **2019**, *25*, 323. (e) Rahman, F. -U.; Tzeli, D.; Petsalakis, I. D.; Teodorakopoulos, G.; Ballester, P.; Rebek, Jr., J.; Yu, Y. *J. Am. Chem. Soc.* **2020**, *142*, 5876. (f) Nag, T.; Ovens, J. S.; Bryce, D. L. *Acta Cryst. C*. **2022**, *78*, 517. (g) Ishigaki, Y.; Shimomura, K.; Asai, K.; Shimajiri, T.; Akutagawa, T.; Fukushima, T.; Suzuki, T. *Bull. Chem. Soc. Jpn.* **2022**, *95*, 522.

(10) (a) Klapötke, T. M.; Krumm, B.; Gálvez-Ruiz, J. C.; Nöth, H.; Schwab, I. *Eur. J. Inorg. Chem.* **2004**, 4764. (b) Klapötke, T. M.; Krumm, B.; Scherr, M. *Inorg. Chem.* **2008**, *47*, 7025. (c) Martínez, Y. B.; Pirani, L. S. R.; Erben, M. F.; Boese, R.; Reuter, C. G.; Vishnevskiy, Y. V.; Mitzel, N. W.; Della Védova, C. O. *ChemPhysChem* **2016**, *17*, 1463. (d) Martínez, Y. B.; Pirani, L. S. R.; Erben, M. F.; Boese, R.; Reuter, C. G.; Vishnevskiy, Y. V.; Mitzel, N. W.; Védova, C. O. D. *J. Mol. Struct.* **2017**, *1132*, 175. (e) Previtali, V.; Sánchez-Sanz, G.; Trujillo, C. *ChemPhysChem* **2019**, *20*, 3186.

(11) Suzuki, T.; Fujii, H.; Yamashita, Y.; Kabuto, C.; Tanaka, S.; Harasawa, M.; Mukai, T.; Miyashi, T. *J. Am. Chem. Soc.* **1992**, *114*, 3034.

(12) Yamashita, Y.; Suzuki, T.; Mukai, T.; Saito, G. *J. Chem. Soc., Chem. Commun.* **1985**, 1044.

(13) Neidlein, R.; Tran-Viet, D.; Girene, A.; Kokkinidis, M.;Wilckens, R.; Geserich, H.; Rüppel, W. *Chem. Ber.* **1982**, *115*, 2898.

(14) Lehnert, W. *Tetrahedron Lett.* **1970**, *11*, 4723.

(15) Aumüller, A.; Hünig, S. *Liebigs. Ann. Chem.* **1984**, 618

(16) (a) Yamashita, Y.; Suzuki, T.; Saito, G.; Mukai, T. *Chem. Lett.* **1986**, 715. (b) Kobayashi, K.; Gajurel C. L. *J. Chem. Soc., Chem. Commun.* **1986**, 1779. (c) Iwasaki, F.; Toyoda, N.; Hirota, M.; Yamazaki, N.; Yasui M.; Kobayashi, K. *Bull. Chem. Soc. Jpn*. **1992**, *65*, 2173.

(17) Yamashita, Y.; Suzuki, T.; Mukai, T. *J. Chem. Soc., Chem. Commun.* **1987**, *16*, 1184.

(18) Hirayama, M.; Seki, A.; Yamashita, Y.; Suzuki, T. Miyashi, T. *J. Chem. Soc., Chem. Commun.* **1988**, 490.

(19) (a) Schubert, U.; Hünig, S.; Aumüller, A. *Liebigs Ann. Chem.* **1985**, 1216. (b) Kabuto, C.; Fukazawa, Y.; Suzuki, T.; Yamashita, Y.; Miyashi, T.; Mukai, T. *Tetrahedron Lett.* **1986**, *27*, 925. (c) Martín, N.; Hanack, M. *J. Chem. Soc., Chem. Commun.* **1988**, 1522. (d) Suzuki, T.; Ichioka, K.; Higuchi, H.; Kawai, H.; Fujiwara, K.; Ohkita, M.; Tsuji, T.; Takahashi, Y. *J. Org. Chem.* **2005**, *70*, 5592. (e) Gómez, R.; Seoane, C.; Segura, J. L. *Chem. Soc. Rev.* **2007**, *36*, 1305. (f) Bureš, F.; Bernd Schweizer, W.; Boudon, C.; Gisselbrecht, J. -P.; Gross, M.; Diederich, F. *Eur. J. Org. Chem.* **2008**, 994. (g) Chiba, H.; Nishida, J.; Yamashita, Y. *Chem. Lett.* **2012**, *41*, 482.

(20) Kabuto, C. ; Suzuki, T.; Yamashita, Y.; Mukai, T. *Chem. Lett.* **1986**, *15*, 1433.

(21) Ishigaki, Y.; Shimajiri, T.; Suzuki, T. to be submitted.

(22) Suzuki, T.; Kabuto, C.; Yamashita, Y.; Saito, G.; Mukai, T.; Miyashi, T. *Chem. Lett.* **1987**, *16*, 2285.

(23) Suzuki, T.; Kabuto, C.; Yamashita, Y.; Mukai, T.; Miyashi, T.; Saito, G. *Bull. Chem. Soc. Jpn*. **1988,** *61*, 483.

(24) Romito, D.; Fresta, E.; Cavinato, L. M.; Kählig, H.; Amenitsch, H.; Caputo, L.; Chen, Y.; Samorì, P.; Charlier, J.-C.; Costa, R. D.; Bonifazi, D. *Angew. Chem. Int. Ed.* **2022**, 61, e202202137.

(25) Yamashita, Y.; Suzuki, T.; Saito, G.; Mukai, T. Chem. Lett. 1985, 14, 1759.

(26) (a) Ugawa, A.; Iwasaki, K.; Kawamoto, A.; Yakushi, K.; Yamashita, Y.; Suzuki, T. *Phys. Rev. B* **1991**, *43*, 14718. (b) Iwasaki, K.; Ugawa, A. Kawamoto, A.; Yamashita, Y.; Yakushi, K.; Suzuki, T.; Miyashi, T. *Bull. Chem. Soc. Jpn*. **1992**, *65*, 3350.

(27) Suzuki, T.; Kabuto, C.; Yamashita, Y.; Mukai, T.; Miyashi, T.; Saito, G. *Bull. Chem. Soc. Jpn*. **1987**, *60*, 2111.

(28) Suzuki, T.; Kabuto, C.; Yamashita, Y.; Mukai, T.; Miyashi, T. *J. Chem. Soc., Chem. Commun.* **1988**, 895.

(29) Suzuki, T.; Fukushima, T.; Yamashita, Y.; Miyashi, T. *J. Am. Chem. Soc.* **1994**, *116*, 2793.

(30) Recent review: Fan Hu, F,; Bi, X.; Chen, X.; Pan, Q.; Zhao, Y. *Chem. Lett.* **2021**, *50*, 1015.

(31) Koshima, H. *J. Mol. Struc.* **2000**, *552.* 111.

(32) Reviews: (a) Sakamoto, M. *Chem. Eur. J.* **1997**, *3*, 684. (b) Sakamoto, M. *J. Photochem. Photobiol., C Photochem. Rev.* **2006**, *7*, 183.

(33) Suzuki, T.; Fukushima, T.; Miyashi, T.; Tsuji, T. *Angew. Chem. Int. Ed. Engl.* **1997**, *36*, 2495.
(34) Fukushima, T.; Okazeri, N.; Miyashi, T.; Suzuki, K.; Yamashita, Y.; Suzuki, T. *Tetrahedron Lett.* **1999**, *40*, 1175.
(35) Review: Biedermann, P. U.; Stezowski J. J.; Agranat , I. *Eur. J. Org. Chem.* **2001**, 15.
(36) (a) Meyer, H. *Monatsh. Chem.* **1909**, *30*, 165. (b) Meyer, H. *Ber. Dtsch. Chem. Ges.* **1909**, *42*, 143.
(37) (a) Hirao, Y.; Hamamoto, Y.; Nagamachi, N.; Kubo, T. *Phys. Chem. Chem. Phys*, **2019**, *21*, 12209. (b) Hamamoto, Y.; Hirao, Y.; Kubo, T. *J. Phys. Chem. Lett.* **2021**, *12*, 19, 4729.
(38) (a) Biedermann, P. U.; Stezowski J. J.; Agranat , I *Chem. Eur. J.* **2006**, *12*, 3345. (b) Takezawa, H.; Murase, T.; Fujita, M. *J. Am. Chem. Soc.* **2012**, *134*, 17420. (c) Matsuo, Y.; Wang, Y.; Ueno, H.; Nakagawa, T.; Okada, H. *Angew. Chem. Int. Ed.* **2019**, *58*, 8762. (d) Wang, Y.; Ma, Y.;Ogumi, K.; Wang, B.; Nakagawa, T.; Fu. Y.; Matsuo, Y. *Commun. Chem..* **2020**, *3*, 93. (e) Sugawara, K.; Ono, T. ; Yano, Y.; Suzuki, T.; Ishigaki, Y. *Mater. Chem. Front.* **2023**, in press [DOI: 10.1039/D2QM01199A].
(39) (a) Suzuki, T.; Yamashita, Y.; Kabuto, C.; Miyashi, T. *J. Chem. Soc., Chem. Commun.* **1989**, 1102. (b) Suzuki, T.: Yamashita, Y.; Fukushima, T.; Miyashi, T. *Mol. Cryst. Liq. Cryst.* **1997**, 296, 165.
(40) Tsubata, Y.; Suzuki, T.; Yamashita, Y.; Mukai, T.; Miyashi, T. *Heterocycles* **1992**, *33*, 337.
(41) Peluso, P.; Dessì, A.; Dallocchio, R.; Sechi, B.; Gatti, C.; Chankvetadze, B.; Mamane, V.; Weiss, R.; Pale, P.; Aubert, E.; Cossu, S. *Molecules* **2021**, 26, 221.
(42) (a) Suzuki, T.; Kabuto, C.; Yamashita, Y.; Mukai, T. *Chem. Lett.* **1987**, *16*, 1129. (b) Ishigaki, Y.; Asai, K.; Shimajiri, T.; Akutagawa, T.; Fukushima, T.; Suzuki, T. *Org. Mater.* **2021**, *3*, 90.
(43) shigaki, Y.; Asai, K.; Jacquot de Rouville, H.-P.; Shimajiri, T.; Heitz, V.; Fujii-Shinomiya, H.; Suzuki T. *Eur. J. Org. Chem.* **2021**, 990.
(44) Someya, T.; Sekitani, T.; Iba, S.; Kato, Y. ; Kawaguchi, H.; Sakurai, T. *Proc. Nat. Acad. Sci.* **2004**, *101*, 9966-9970.
(45) (a) Kim, S. J. *Appl. Chem .Eng.* **2018**, *29*, 799. (b) Ban, H.; Cheng, Y.; Wang, L.; Li, X.; Zhou, X.; Zhang, X. *Chem. Eng. Technol.* **2019**, *42*, 1188.
(46) Fujii, S.; Koike, M.; Nishino, T.; Shoji, Y. ; Suzuki, T.; Fukushima, T.; Kiguchi, M. *J. Am. Chem. Soc.* **2019**, 1*14,* 18544.
(47) Murase, R.; Hudson, T. A.; Aldershof, T. S.; Nguyen, K. V.; Gluschke, J. G.; Kenny, E. P.; Zhou, X.; Wang, T. ; van Koeverden, M. P.; Powell, B. J.; Micolich, A. P.; Abrahams, B. F.; D'Alessandro, D. M. *J. Am. Chem. Soc.* **2022**, *144*, 13242.
(48) Ishigaki, Y.; Asai, K.; Shimajiri, T.; Suzuki, T. *Chem. Lett.* **2021**, *50*, 1184.
(49) Scheiner, S. *ChemPhysChem* **2023**, in press (DOI: 10.1002/cphc.202200936)